

Synthesis of modified nanocomposite material and its use on removal of cesium from aqueous media

Bilal ÇETİN^{1*}, Mustafa ÖZCAN², Bektaş KARAKELLE¹

¹Turkish Energy Nuclear and Mineral Agency, İstanbul, Turkey

²Department of Chemistry, Faculty of Science and Letters, İstanbul Technical University, İstanbul, Turkey

Received: 26.05.2021 • Accepted/Published Online: 24.08.2021 • Final Version: 23.02.2022

Abstract: A nanocomposite containing Fe_3O_4 , chitosan (Ch), and hexacyanoferrate (HCF) was synthesized in the form of powder. The physicochemical properties of this nanocomposite are determined using different techniques including Fourier transform infrared spectroscopy (FTIR), X-ray diffraction (XRD), thermogravimetric analysis (TGA), scanning electron microscopy (SEM). The existence of Cs (Cs) ions onto the surface of the nanocomposite was verified by dispersive X-ray spectroscopy (EDX). FTIR spectra confirmed that the nanocomposite was well coordinated. The batch technique was applied to evaluate the influences of initial pH value, temperature, contact time, shaking rate, initial Cs concentration, and competing cations on the efficiency of Cs removal. The maximum adsorption capacity for Cs ions of nanocomposite was determined as 34.36 mg/g at the initial pH = 5 of the aqueous solution. The equilibrium data fitted well the linearized Langmuir isotherm equation, which has the higher correlation coefficient (0.999). Thermodynamic parameters such as free energy (ΔG°), enthalpy (ΔH°), and entropy (ΔS°) indicated that the adsorption was exothermic and not spontaneous.

Key words: Cs, Fe_3O_4 , chitosan, adsorption, hexacyanoferrate, nanocomposite

1. Introduction

Radioactive waste (RW) is an inevitable residue from the use of radioactive materials (RMs) in industry and the medical sector, as well as from research and nuclear establishments. The management and disposal of such RW is, therefore, an issue relevant to almost all countries. Also, the development of nuclear science and technology, in particular the wide application of nuclear power, seriously threatens the human environment through radioactivity contamination. Two of the most important fission radionuclides from the reactor, ^{137}Cs and ^{134}Cs , are considered potentially dangerous to human health and to the environment because the relatively high yield in nuclear power plants, long half lives, and high solubility of Cs (Cs) can cause its migration through groundwater to the biosphere [1]. In other respects, they can be easily adsorbed by terrestrial and aquatic organisms, because of their chemical similarity to potassium (K). The formation of complexes does not have a significant effect on Cs speciation, and the predominant aqueous species in groundwater is the free Cs ion [2]. Different techniques, such as solvent extraction, evaporation, and ion exchange, are usually used for the treatment of aqueous waste solutions containing Cs ion [3–4].

Recently, considerable attention has been paid to the synthesis of nanocrystalline materials (NMs) to increase their industrial applications, owing to their large surface area and shorter diffusion paths compared to the micro sized crystals (MSC) [5]. In spite of its benefits, there is a problem related to the separation of spent nanomaterials from the aqueous medium. The technique for the former's separation involves the use of centrifugation process, which is very costly and time consuming. Lately, researchers proceeded to use the magnetic separation technique (MST) since it is efficient, simple, and fast [6]. Magnetic nanoparticles (MNs), which are composed of a MN based core and a functional shell that can adsorb contaminants, such as heavy metals or radioactive nuclides have been intensively analyzed for environmental remediation applications due to their high surface areas and ability to be magnetically collected using an external magnet [7,8]. Fe_3O_4 has low toxicity and is small in size. Magnetization of adsorbent matrix facilitates separation of the used sorbent [9].

Chitosan (Ch) is a biopolymer obtained by the deacetylation of chitin [10–12]. Moreover, metal nanoparticles can be incorporated with Ch to form a composite [13]. Ch has an excellent adsorption capacity for various metals, such as Cr(VI), Cu(II), Pt(IV), Pd(II), Co(II), Ni(II), and Fe(III). Metal uptake by Ch is primarily attributed to the hydroxyl

* Correspondence: bilal.cetin@tenmak.gov.tr

and amine groups existing in the polymer chain, the functional groups can react with the different metallic species through the mechanism of chelation and/or ion exchange [14]. Ch has two hydroxyl groups and one amino group on each glucosamine monomer, the amino groups can be strongly linked to metal ions, and amino and hydroxyl groups can be interactive with organic compounds via hydrogen bonding. At the same time, the amino group of Ch is easily protonated in acidic solutions, restricting the application in the adsorption process [15].

Different sorbents modified with Ch have been used for heavy metal removal such as chitosan-tripolyphosphate beads, chitosan-cellulose hydrogel beads, chitosan-graft- γ -cyclodextrin, tetraethylenepentamine modified magnetic chitosan resin, Guar Gum/Magnetite/Chitosan, magnetic Schiff's base chitosan composite, chitosan-clay, chitosan-inorganics etc. Rough range of metal sorption capacity by chitosan-based sorbents have been varied between 4.1 mg/g and 3170 mg/g for heavy metal removal [16-19].

Metal hexacyanoferrate (MHCF) analogues are the inorganic complexes known for their versatile applications [20]. Transition metal hexacyanomethylates (TMHCM) usually have an open channel framework appropriate for small molecules separation, and their crystal structure is closely related to the coordination adopted by the metal centers. In hexacyanomethylates (HCMs), the involved transition metals (TM) are usually found with octahedral coordination within the cubic unit cell (Fm-3m). Some zinc hexacyanoferrates (ZnHCF) have been reported as hexagonal where Zn^{2+} atom is found tetrahedrally coordinated to four nitrogen (N) atoms from cyano (CN) ligands. Such coordination provides a relatively high thermal stability to these materials and also an interesting porous framework because both metal centers have saturated their coordination sphere with atoms from the bridge group (-CRN-) [21].

In the present work, Fe_3O_4 was synthesized from iron ore waste and used to form the nucleus of the nanocomposite adsorbent. Later, nanocomposite containing chitosan and metal hexacyanoferrate was synthesized using Fe_3O_4 . The synthesized adsorbent was characterized and used to determine optimum adsorption parameters such as initial pH value, temperature, contact time, shaking rate, initial Cs concentration, adsorbent amount. The results obtained were used to determine the adsorption type, isotherms, adsorption capacity, and thermodynamic values.

2. Experimental

2.1. Materials

Iron ore waste used in obtaining of Fe_3O_4 was supplied by Kroman Çelik Sanayii A.S. (Istanbul, Turkey). The chitosan compound was purchased from İsmail Aslan Chemistry (Sakarya, Turkey), $K_4Fe(CN)_6 \cdot 3H_2O$ (HCF) was purchased from Merck KGaA (Darmstadt, Germany), other chemicals are analytical grade and used as received without additional processing.

2.2. Preparation of composite

2.2.1. Synthesis of magnetic nanoparticles Fe_3O_4

A total of 25 g of iron ore waste was taken and treated with 90 mL of HCl acid at 90 °C for 6 h. Insoluble particles filtered from the mixture were brought to room temperature by means of blue band filter paper, and this filtrate containing Fe (III) was diluted to 250 mL (Stock A) and maintained under pH = 1. A total of 100 mL of stock a solution was taken and Fe (III) was reduced to Fe^0 in the form of black iron particles by mixing with $NaBH_4$ in an ice-cold water bath quickly. $NaBH_4$ was added until the solution became colorless. The solution containing metallic iron was filtered through blue band filter paper to obtain black iron particles, first washed with ethanol and then with distilled water twice. The resulting metallic iron was added to 100 mL of Stock A solution and a Fe (II) solution (Stock B) was obtained. Fe amount in Stock A and Stock B was determined by ICP-OES (Perkin Elmer-Optima 8000). Aliquots were taken from stock A and Stock B solutions with a Fe^{3+}/Fe^{2+} molar ratio of 2:1 and placed an erlenmeyer. 25% NH_3 was added at room temperature until the mixture had a pH value of 10, and then Fe_3O_4 was precipitated. The mixture was filtered after the magnetic properties of the compound obtained are checked by an external magnet. Fe_3O_4 was washed three times with pure water and dried for one day at 60 °C in the oven.

2.2.2. Synthesis of Fe_3O_4 /Chitosan composite

0.6 g chitosan was dissolved in 15 mL (2% v/v) acetic acid with vigorous stirring for 1 h. Aliquots from Stock A and Stock B solutions were taken with a Fe^{3+}/Fe^{2+} molar ratio of 2:1 and added to the mixture containing chitosan. The entire mixture was stirred for 2 h until a dark red viscous mixture was obtained. The above-mentioned mixture was added to 1.3 M 50 mL NaOH solution and stirred for 12 h at room temperature. The precipitate formed was filtered and washed with distilled water. All these processes were carried out in an inert N_2 atmosphere to prevent Fe^{2+} oxidation. The precipitate was dispersed in 30 mL (20% w/v) sodium tripolyphosphate (STPP) solution and mixed for 2 h. The mixture was filtered, and the precipitate was washed in distilled water and ethanol, respectively, and then dried at 60 °C for one day. The composite shows whether the magnetic properties were checked with the help of an external magnet.

2.2.3. Synthesis of Fe₃O₄/Ch/HCF composite

Fe₃O₄/Chitosan was added to 0.1 M K₄Fe(CN)₆·3H₂O solution and stirred for 3 h in N₂ atmosphere. Then, 0.1 M ZnCl₂ was slowly added dropwise in an inert N₂ atmosphere and stirred for 3 h. The precipitate was filtered and recrystallized in a 3:2 isopropyl alcohol-acetone mixture, then washed 3-4 times with distilled water and allowed to dry at room temperature. After the composite obtained was pulverized, it was sieved in a 38 micron-sized sieve and kept in an airtight container.

2.3. Adsorption experiments

The batch technique was used to adsorb Cs onto nanocomposite adsorbent. A total of 100 mg/L Cs⁺ stock solution prepared, and adsorption experiments were carried out in Memmert-WNB 29 model temperature-controlled shaking water bath by taking aliquots from this stock solution. pH studies between 2 and 10, temperature studies between 25 °C and 60 °C, adsorbent amount studies between 10 mg and 100 mg, contact time studies between 30 min and 300 min, shaking rate studies between 80 rpm and 180 rpm, initial Cs concentration studies between 2.5 mg/L and 80 mg/L were performed. After the adsorption experiments, the Cs concentration in the supernatant obtained was determined by the flamed atomic emission spectrometer (Varian Spectr AA 200, 852.7 nm wavelength, slit: 1.0 nm, 2000 mg/L Potassium (K) ionization suppressor) with air/acetylene. The adsorption capacity q_e (mg/g) in equilibrium was calculated using the following equation:

$$q_e = \frac{(C_0 - C_e)V}{W} \quad (1)$$

where C_0 ; Initial concentration (mg/L), C_e ; Concentration in equilibrium (mg/L), V ; Solution volume (L), W ; adsorbent weight (g).

Jeol brand JSM 639OLV model scanning electron microscope (SEM) for determining the morphology of Fe₃O₄/Ch/HCF composite, Quantachrome brand Nova 2200e model BET analyzer for determining the surface area, Olympus brand Delta XRF device for determining the Fe amount in the different iron ore wastes were used and Netzsch Brand STA 449C model device was used for DTA and TGA.

3. Results and discussion

3.1. Characterization

3.1.1. SEM images

SEM image of pure chitosan, Fe₃O₄/Ch and Fe₃O₄/Ch/HCF composite is given in Figure 1. As can be seen from the image, nanocomposite does not have a specific shape and the size of the particles varies between 1 µm and 25 µm. EDX analysis (Figure 2) was performed to determine the elemental composition of composite and whether Cs adsorption was performed, and the results are presented in Table 1. There is no Cs in the structure of the composite before adsorption, but, when the results of EDX spectrum after the adsorption are examined, the presence of Cs is determined, and these data prove that Cs adsorption occurs on the composite.

3.1.2. BET and XRD diffraction

As a result of the BET analysis, the surface area of 1 g of the composite was determined as 60.87 m². XRD analysis was carried out to determine the crystal size of the composite and to determine Fe₃O₄, Chitosan, and HCF in its structure. XRD patterns are shown in Figure 3. Deby-Scherrer equation used in calculating the crystal size of materials is expressed as follows:

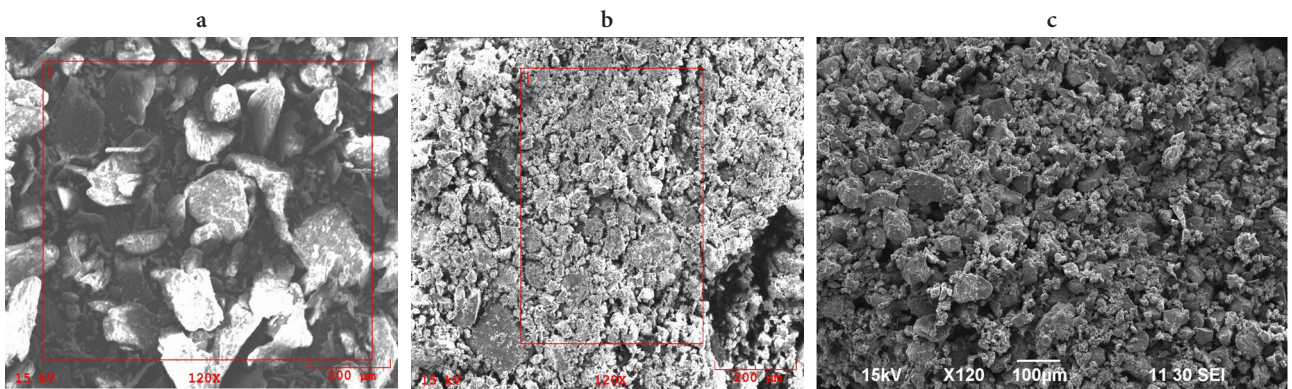


Figure 1. SEM image of (a) pure chitosan, (b) Fe₃O₄/Ch and (c) Fe₃O₄/Ch/HCF nanocomposite.

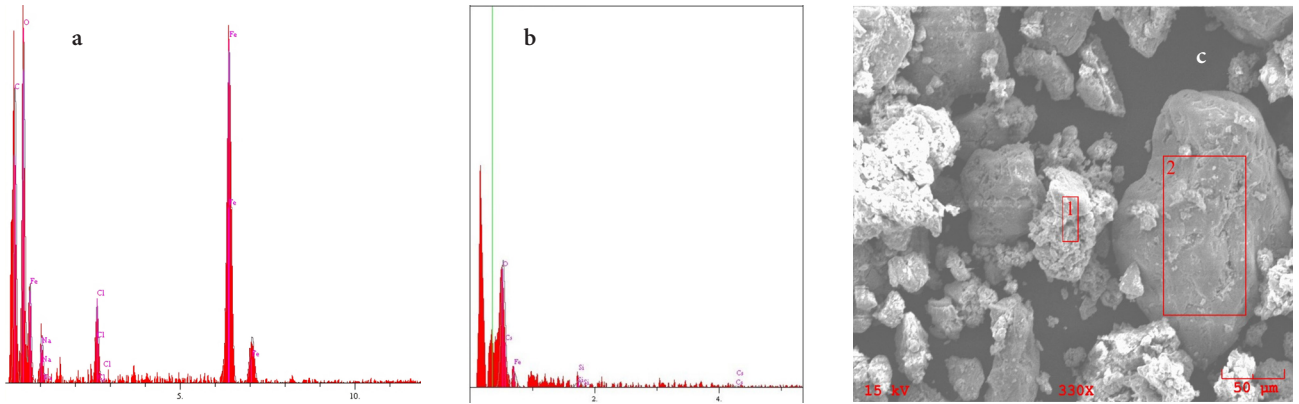


Figure 2. EDX graph of Fe₃O₄/Ch/HCF nanocomposite (a) before Cs adsorption and (b) after Cs adsorption and (c) SEM image of Cs adsorbed Fe₃O₄/Ch/HCF nanocomposite.

Table 1. EDX result of Fe₃O₄/Ch/HCF nanocomposite before and after Cs adsorption.

Elt.	Line		Intensity (c/s)	Error 2-sig	Conc.	Units
C	Ka	Before Adsorption	18.44	0.86	26.18	wt.%
		After Adsorption	7.00	0.53	12.54	wt.%
O	Ka	Before Adsorption	19.73	0.89	21.12	wt.%
		After Adsorption	21.13	0.92	22.84	wt.%
Fe	Ka	Before Adsorption	35.32	1.19	47.62	wt.%
		After Adsorption	36.02	1.20	62.43	wt.%
Cs	La	Before Adsorption	-	-	-	wt.%
		After Adsorption	0.61	0.16	0.98	wt.%

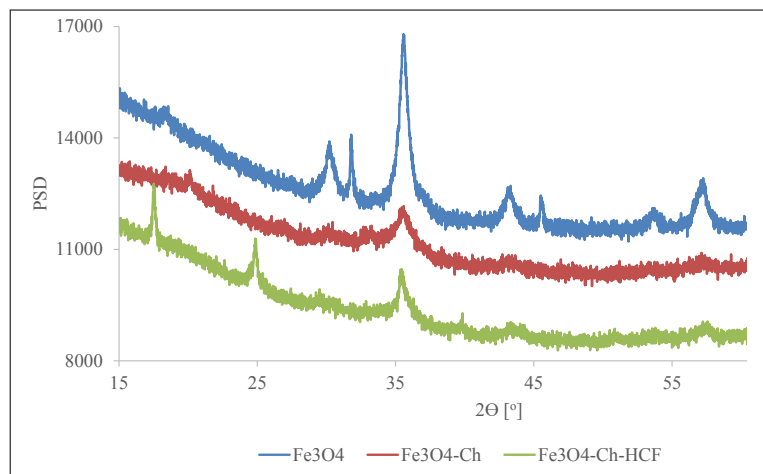


Figure 3. Fe₃O₄, Fe₃O₄/Ch and Fe₃O₄/Ch/HCF XRD patterns.

$$L = \frac{K\lambda}{\beta \cos\theta} \quad (2)$$

where L is the average crystal size, K is the constant about crystal shape, λ is the X-ray wavelength (nm), β is the peak width of the diffraction peak profile at half maximum height due to the small crystal size (rad), and θ is half of the Bragg Angle.

In the calculation made using the Deby-Scherrer equation, the particle size of Fe_3O_4 , which composes the composite, has been calculated as 12.315 nm, and it has been determined that the composite is nanocomposite because it is a nano-sized component. When the XRD patterns of Fe_3O_4 , $\text{Fe}_3\text{O}_4/\text{Chitosan}$, and $\text{Fe}_3\text{O}_4/\text{Ch}/\text{HCF}$ are compared to each other, similar peaks are seen at 35, 56, and 63 2θ positions, which proves to us that there is Fe_3O_4 in the structure of the nanocomposite. Since there are no sharp peaks in the XRD graph of chitosan, it is not possible to compare it with the XRD graph of nanocomposite.

3.1.3. FTIR spectrum

FTIR spectrum of nanocomposite, Chitosan and HCF is given in Figure 4. The peak at 2051 cm^{-1} corresponds to the functional group $-\text{C}\equiv\text{N}$ in the structure $\text{K}_4[\text{Fe}(\text{CN})_6]$ and easily can be seen from the FTIR spectrum of pure HCF. It is understood from the graph that this peak is quite sharp and prominent. Therefore, the presence of $\text{K}_4[\text{Fe}(\text{CN})_6]$ in the structure of the nanocomposite material has been proven. In addition, 1623 cm^{-1} , 1553 cm^{-1} peaks in the structure of Chitosan correspond to N-Acetyl group, 1149 cm^{-1} peak corresponds to C-O-C bridge, 1062 cm^{-1} and 1026 cm^{-1} peaks correspond to C-O stretching and 3261 cm^{-1} peak corresponds to NH, OH, and intermolecular H bonds. All of abovementioned peaks related to Chitosan from the FTIR spectrum of nanocomposite can be easily seen from the FTIR spectrum of pure Chitosan, and all of these abovementioned peaks are proof of the presence of chitosan in the nanocomposite. When we examine the FTIR spectrum of Cs adsorbed- $\text{Fe}_3\text{O}_4/\text{Ch}/\text{HCF}$ nanocomposite the peak at 2051 cm^{-1} in corresponds to the functional group $-\text{C}\equiv\text{N}$ is shifted to 2036 cm^{-1} as well as 3261 cm^{-1} peak corresponds to NH is shifted to 3189 cm^{-1} . These observations show that NH and $-\text{C}\equiv\text{N}$ functional groups of nanocomposites play significant role on Cs adsorption on nanocomposite.

3.1.4. Thermal curves

TGA and DTA plots of $\text{Fe}_3\text{O}_4/\text{Ch}/\text{HCF}$ nanocomposite are shown in Figure 5. According to the DTA result given for chitosan in the literature, it was stated that the decaying peak of the chitosan is exothermic and occurs between $270\text{--}337\text{ }^\circ\text{C}$. The reason for this has been shown to cause thermal degradation of amino and N-acetyl groups [22]. When $\text{Fe}_3\text{O}_4/\text{chitosan}$ nanocomposite was heated up to $200\text{ }^\circ\text{C}$ at room temperature, its mass decreased as a result of evaporation of the adsorbed water in the nanocomposite. Mass loss between $200\text{ }^\circ\text{C}$ and $400\text{ }^\circ\text{C}$ is thought to result from the degradation of chitosan cross-links in the nanocomposite [23].

When the results with TGA and DTA were compared with the literature, it was understood that the mass loss was experienced due to the removal of the adsorbed water molecules between 0 and $200\text{ }^\circ\text{C}$ and the decay of chitosan between 200 and $400\text{ }^\circ\text{C}$. It is determined that the DTA curve is endothermic between 0 and $200\text{ }^\circ\text{C}$, and it is caused by degraded water molecules, and DTA curve is exothermic between $200\text{--}400\text{ }^\circ\text{C}$ because of the degradation of chitosan.

3.2. Adsorption experiment

3.2.1. Effect of initial pH value

Effect of initial pH on adsorption of Cs on nanocomposite is shown in Figure 6. The concentration of Cs is 2.5 mg/L , Cs solution amount is 50 mL , the amount of adsorbent is 10 mg , the temperature is $25\text{ }^\circ\text{C}$, the contact time is 30 minutes, the shaking rate is kept at 125 rpm , and initial pH values are changed between $2, 4, 6, 7, 8$ and 10 . As can be seen in Figure 6, an increase in adsorption between $\text{pH} = 2$ and $\text{pH} = 4$ has been observed and reached the maximum value, no significant pH value changes between 4 and 10 have been observed. Therefore, the optimum initial pH value was chosen as 5 , which is the pH value of the solution.

3.2.2. Effect of temperature

The temperature effect on adsorption of Cs on nanocomposite is shown in Figure 7. The concentration of Cs is 2.5 mg/L , Cs solution amount is 50 mL , initial $\text{pH} = 5$, the amount of adsorbent is 10 mg , the contact time is 30 minutes, the shaking rate is kept at 125 rpm the temperature values are changed between $25, 30, 40, 50$ and $60\text{ }^\circ\text{C}$. As can be seen from Figure 7, the maximum adsorption occurred at $25\text{ }^\circ\text{C}$.

3.2.3. Effect of adsorbent amount

The effect of adsorbent amount on adsorption of Cs on nanocomposite is shown in Figure 8. Cs concentration is 2.5 mg/L , initial $\text{pH}: 5$, Cs solution amount is 50 mL , the temperature is $25\text{ }^\circ\text{C}$, contact time is 30 min , shaking rate is kept at 125 rpm and adsorbent amounts are changed $10, 20, 30, 40, 50, 70,$ and 100 mg , respectively. As can be seen from Figure 8, the maximum adsorption occurred at 50 mg .

3.2.4. Effect of contact time

The effect of contact time on the adsorption of Cs on nanocomposite is shown in Figure 9. Cs concentration is 2.5 mg/L , Cs solution amount is 50 mL , initial $\text{pH} = 5$, temperature is $25\text{ }^\circ\text{C}$, the adsorbent amount is 50 mg , shaking rate is kept at

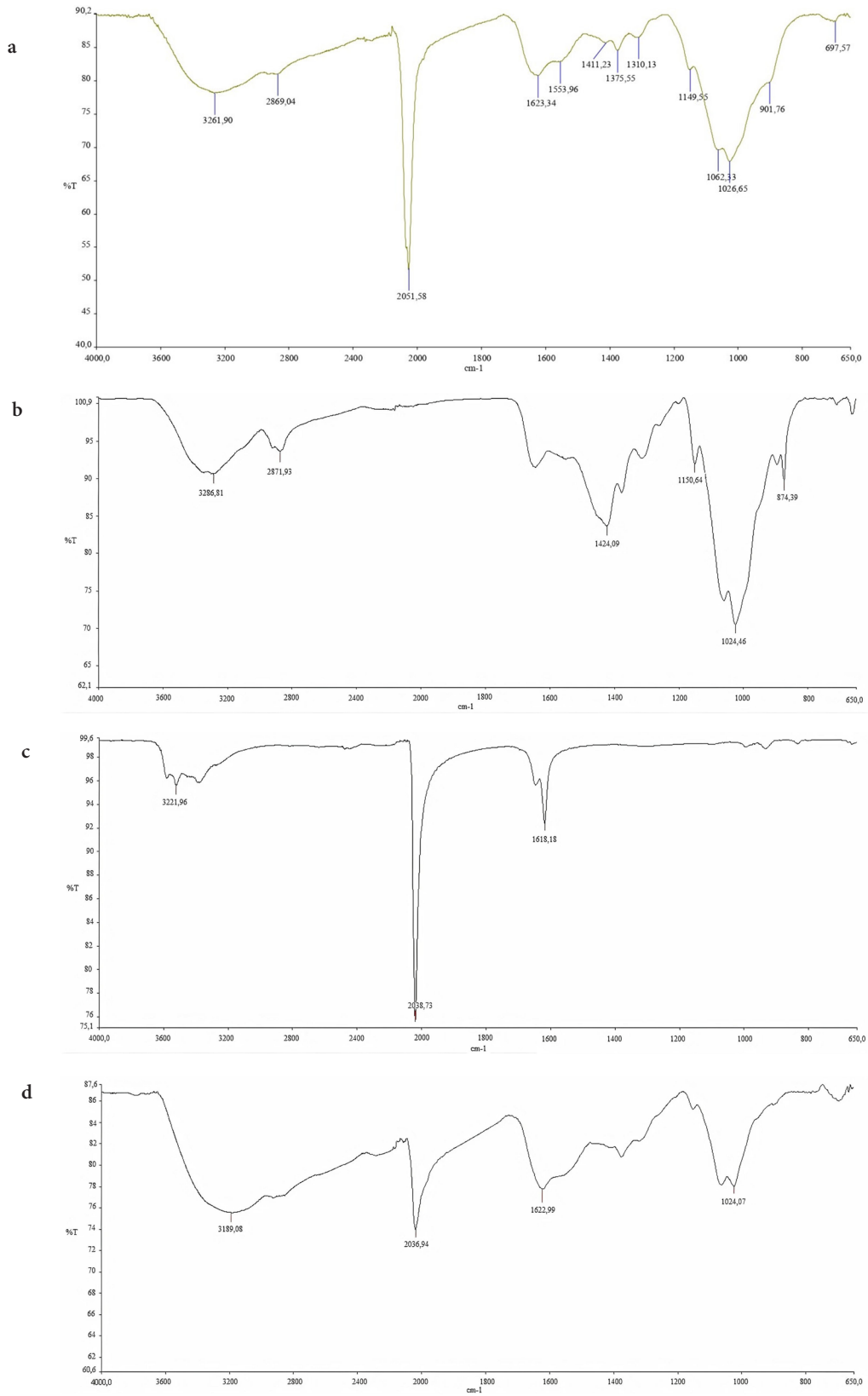


Figure 4. FTIR spectrum of (a) Fe₃O₄/Ch/HCF nanocomposite, (b) Chitosan and (c) HCF and (d) Cs adsorbed- Fe₃O₄/Ch/HCF.

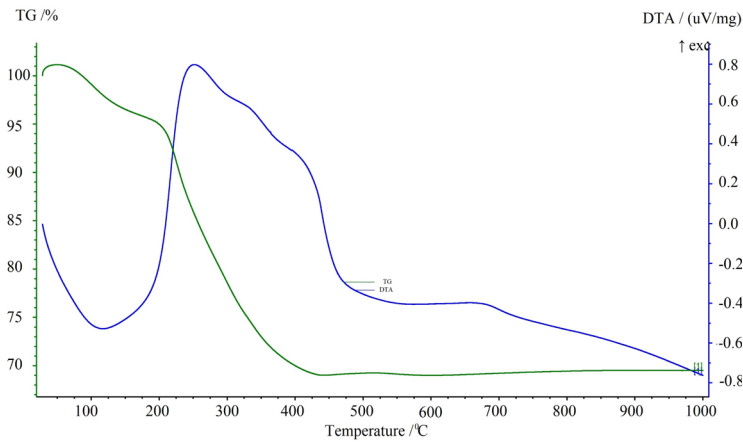


Figure 5. TGA (Green line) and DTA (Blue line) plot of $\text{Fe}_3\text{O}_4/\text{Ch}/\text{HCF}$ nanocomposite and chitosan.

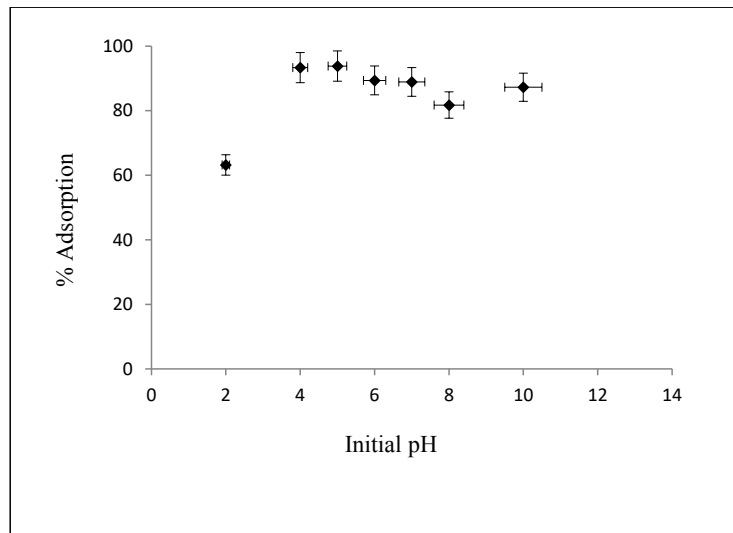


Figure 6. Effect of the initial pH value on Cs adsorption.

125 rpm and contact times are changed 30, 60, 120, 180, 240, and 300 min respectively. As can be seen from Figure 9, the maximum adsorption occurred in 30 minutes.

3.2.5. Effect of initial Cs concentration

The effect of initial Cs concentration on adsorption of Cs on nanocomposite is shown in Figure 10. Temperature is 25 °C, Cs solution amount is 50 mL, initial pH = 5, adsorbent amount is 50 mg, contact time is 30 min, shaking rate is kept at 125 rpm and initial Cs concentration values changed 2.5, 5, 10, 20, 30, 40, 60, and 80 mg/L, respectively. As can be seen from Figure 10, the maximum adsorption occurred at a concentration of 40 mg/L Cs.

3.2.6. Effect of shaking rate

The effect of shaking rate on adsorption of Cs on nanocomposite is shown in Figure 11. The concentration of Cs is 2.5 mg/L, Cs solution amount is 50 mL, initial pH = 5, the temperature is 25 °C, the amount of adsorbent is 50 mg, the contact time is kept constant in 30 min, and the shaking rate values are changed 80, 125, 140, 150, and 180 rpm, respectively. As understood from Figure 11, the maximum adsorption occurred at 140 rpm.

3.2.7. Adsorption isotherms

Analysis of the equilibrium relationship between adsorbed Cs ions and the adsorbent and the balance data obtained from the experiments is very important in elucidating the adsorption properties of $\text{Fe}_3\text{O}_4/\text{Ch}/\text{HCF}$ nanocomposite adsorbent. Adsorption equilibrium data obtained at different Cs concentrations (2.5–80 mg/L) and at different temperatures (25–60

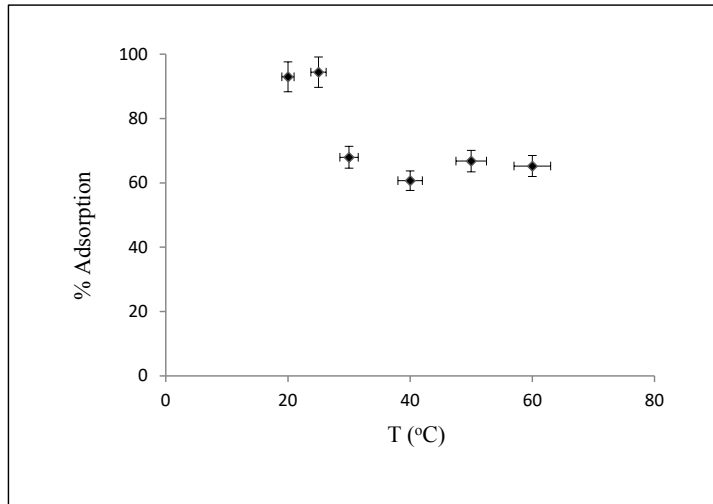


Figure 7. Effect of temperature on Cs adsorption.

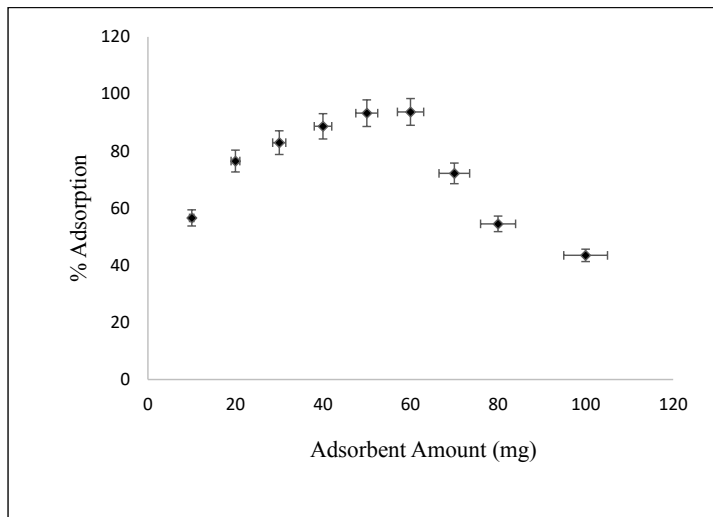


Figure 8. Effect of adsorbent amount on Cs adsorption.

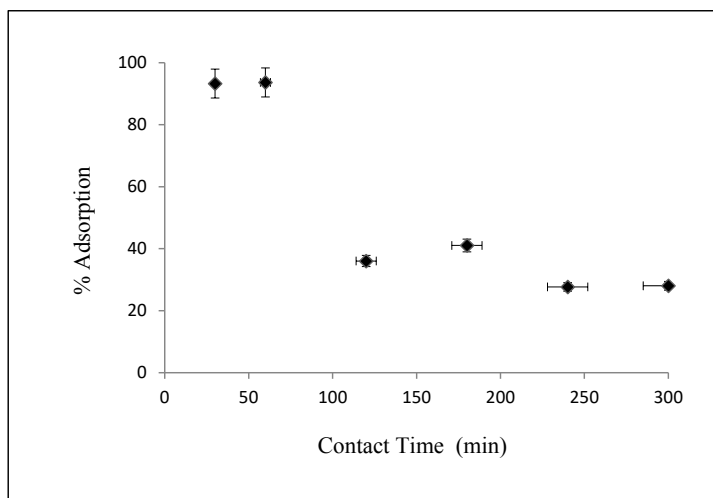


Figure 9. Effect of contact time on Cs adsorption.

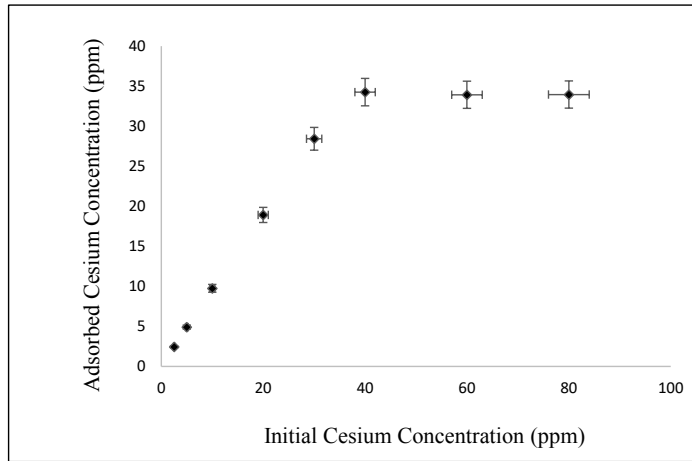


Figure 10. Effect of initial Cs concentration on Cs adsorption.

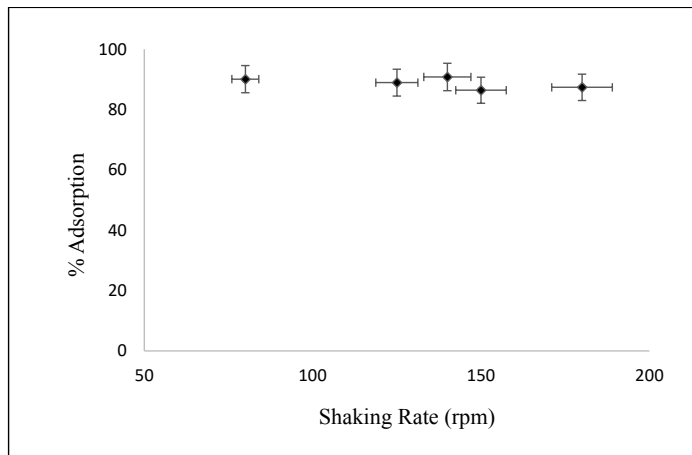


Figure 11. Effect of shaking rate on Cs adsorption.

°C) were applied in the Langmuir and Freundlich isotherm models, and the equations for these isotherms are expressed, respectively, as follows:

$$q_e = \frac{q_{max}K_l C_e}{1 + K_l C_e} \quad (3)$$

$$q_e = K_f C_e^{1/n} \quad (4)$$

where C_e is equilibrium concentration of Cs in solution (mg/L), q_e is adsorption capacity of adsorbent in equilibrium (mg/g) q_{max} is adsorbent's maximum adsorption capacity, K_l is Langmuir equilibrium constant (L/mg), K_f is Freundlich equilibrium constant (L/mg).

Graphs of Freundlich and Langmuir isotherms obtained from cesium adsorption balance data are given in Figure S1. and Figure S2. at the supplementary materials, respectively. The maximum adsorption capacities, error values calculated by sum of squared error (SSE), and adsorption constants obtained from Freundlich and Langmuir isotherm models in Cs adsorption on nanocomposite are presented in Table 2. As seen in Table 2, when the correlation coefficient values (R^2) of Cs ions on adsorption of $Fe_3O_4/Ch/HCF$ on nanocomposite adsorbent and error values (SSE) were examined, Langmuir isotherm model was observed to fit better than Freundlich model and maximum adsorption capacity was determined as 34.36 mg/g.

Table 2. Comparison of Freundlich and Langmuir constants.

Model	Adsorbent	Cs(I)			
		q	K_L	R ²	SSE
Langmuir	Fe ₃ O ₄ /Ch/HCF	3	2.01	0.999	36.34
Freundlich		K	1/n	R ²	SSE
		1	0.363	0.831	769.28

As a result of fit to the Langmuir isotherm model of the adsorption of Cs ions on Fe₃O₄/Ch/HCF nanocomposite adsorbent, It can be concluded that the adsorption surface is homogeneous and adsorption occurs in a single layer on the surface, the adsorption is localized and the adsorbed ions do not move on the surface, the adsorption enthalpy is independent from the surface coating, there are no interactions between adsorbed ions, and the amount of substance adsorbed per unit surface has no effect on the adsorption rate.

3.2.8. Adsorption mechanism

It is stated that chitosan interacted with iron ions and hydroxyl groups on the surface of Fe₃O₄ by means of functional amino groups. The iron oxide nuclei form iron oxide aggregates and iron oxide polycrystalline nanostructures are formed on the surface of these aggregates by self-assembly; thus, it was concluded that the synthesized structure is in the form of mesopore structure [24]. Amino groups in the structure of chitosan are protonated as -NH³⁺ in acidic environments, and chitosan has a good chelating feature, because of the presence of N atom in amino groups that can be well-coordinated with ions with empty orbitals such as Fe²⁺ and Fe³⁺ [25]. It has been stated that chitosan is polycationic when dissolved in acid and it presents -NH³⁺ regions. Sodium tripolyphosphate (Na₃P₃O₁₀) is mentioned that when it dissolves in water, it decomposes into hydroxyl and phosphoric ions. It has been reported that at high pH values, -OH⁻ and P₃O₅⁻ are formed and these ions compete with each other in interaction with the -NH³⁺ regions, and, as a result of deprotonization of -OH⁻ ions, P₃O₅⁻ ions interact with the -NH³⁺ groups of chitosan by ionic cross-linking [26]. Fe₃O₄/Chitosan formation; It is stated that Fe³⁺ ions form chelates on the chitosan chain through amino and hydroxyl groups on chitosan, and the chelating effect of the -NH₂ and -OH groups distributes iron ions homogeneously [23]. Also, the FTIR spectrum of Cs adsorbed- Fe₃O₄/Ch/HCF nanocomposite proves that -C≡N in the structure of K₄[Fe(CN)₆] and -NH₂ the structure of Chitosan plays a significant role in the adsorption of Cs onto nanocomposite.

3.2.9. Thermodynamics of sorption

Adsorption thermodynamics were investigated to further illuminate the effect of temperature on energy changes in Cs adsorption and adsorption process. Changes in adsorption capacity caused by temperature change can be explained based on thermodynamic parameters such as free energy (ΔG°), enthalpy (ΔH°) and entropy (ΔS°). Thermodynamic equations are expressed as follows

$$\Delta G^\circ = -RT(\ln K_e^0) \quad (5)$$

$$\ln\left(\frac{K_L}{Y_e}\right) = -\frac{\Delta H^\circ}{R} \frac{1}{T} + \frac{\Delta S^\circ}{R} \quad (6)$$

$$\Delta G^\circ = \Delta H^\circ - T\Delta S^\circ \quad (7)$$

Here, R is ideal gas constant (8.314 J/molK), T is adsorption temperature (K), K_L is the Langmuir isotherm constant, Y_e is the coefficient of activity for Cs and K_e^0 is the dimensionless thermodynamic equilibrium constant and can be calculated by the equation given below [27]:

$$K_e^0 = \frac{1000 \cdot K_L \cdot \text{Molecular weight of adsorbate} \cdot [\text{adsorbate}]^0}{\gamma} = \frac{K_e}{\gamma} \quad (8)$$

Enthalpy (ΔH°) and entropy (ΔS°) and then free energy (ΔG°) values were calculated from the graph equation obtained by drawing $1/T$ (K⁻¹) values against $\ln K_e^0$ values obtained from temperature effect studies on Cs adsorption. ΔH° value was calculated -21.50 kJ/mol, ΔS° value was calculated 0.081 kJ/molK, ΔG° values at 25 °C, 40 °C and 60 °C were calculated as -45.59, -46.80 and -48.42 kJ/mol, respectively. The adsorption enthalpy (ΔH°) is negative, and the entropy (ΔS°) is positive; due to this reason, the adsorption process is exothermic and spontaneous. The fact that the adsorption enthalpy (ΔH°) is negative and entropy (ΔS°) are positive as well as the free energy (ΔG°) value is also negative indicates that the

adsorption occurs spontaneously at all temperatures. Additionally, Cs adsorption onto nanocomposite adsorbent (Fe₃O₄/Ch/HCF) is occurred physically due to low adsorption enthalpy (ΔH°) which is -21.50 kJ/mol [28].

3.2.10. The effect of competing ions

The effect of competitive ions (Sr²⁺, Co²⁺) on Cs adsorption was investigated. Sr²⁺ and Co²⁺ ions have been selected because radioactive strontium and cobalt isotopes are often found together with the radioactive isotope of Cs in liquid radioactive waste arised from operations, decommissioning, and accidents of reactors. In the aspect of radiological safety, strontium (Sr-90), cobalt (Co-60), and Cs (Cs-137) are major radioactive isotopes because of their relatively long half-lives, high solubility, and transferability [14]. A total of 50 mL solution was prepared in which each ion had a concentration of 40 mg/L. As it can be seen in Table 3, when there is no competitive ion in the solution, adsorption is 85.65%, while this value has decreased to 65.53% in the presence of competitive ions. This may be due to the fact that foreign ions are adsorbed to the surface of the nanocomposite by complexity or nonspecific surface interactions rather than the ion exchange process. Table 3 also shows that Sr²⁺ or Co²⁺ effects, which are separate from each other on Cs adsorption, is almost same.

3.2.11. Desorption studies

Loaded nanocomposites obtained from earlier studies were used to determine the desorption behavior of Cs⁺. Deionised (DI) water, 0.1 M, 0.5 M, and 1 M HCl and 0.1 M, 0.5 M, and 1 M NaOH were used as desorption agents. Loaded nanocomposites (0.05 g each) were transferred to a clean flask containing 50 mL of 0.1 M, 0.5 M, and 1 M HCl, DI water and 0.1 M, 0.5 M, and 1 M NaOH. The mixture was agitated in a rotary shaker at 140 rpm for 30 min. The desorption efficiency is determined by Eq. (9):

$$Desorption \% = \frac{amount\ of\ metal\ ion\ desorbed}{amount\ of\ metal\ ion\ adsorbed} \times 100$$

Figure 12 shows the result of the desorption experiments. NaOH was most effective, causing 91.29% of the adsorbed Cs to desorp. 0.5 M NaOH and 1 M NaOH showed almost same desorption effect. The results suggest that the loaded nanocomposite may be suitable for disposal into designated landfill if it is protected from alkaline leachate [29].

Table 3. Sr²⁺ and Co²⁺ effect on Cs adsorption.

Analyte	Ion	Ion Source	Competitive Ion Conc. (mg/L)	Adsorption %
Cs ⁺	Sr ²⁺ , Co ²⁺	Sr(NO ₃) ₂ , Co(NO ₃) ₂	0	85.65
Cs ⁺	Sr ²⁺ , Co ²⁺	Sr(NO ₃) ₂ , Co(NO ₃) ₂	40	65.53
Cs ⁺	Sr ²⁺	Sr(NO ₃) ₂	40	81,28
Cs ⁺	Co ²⁺	Co(NO ₃) ₂	40	79,23

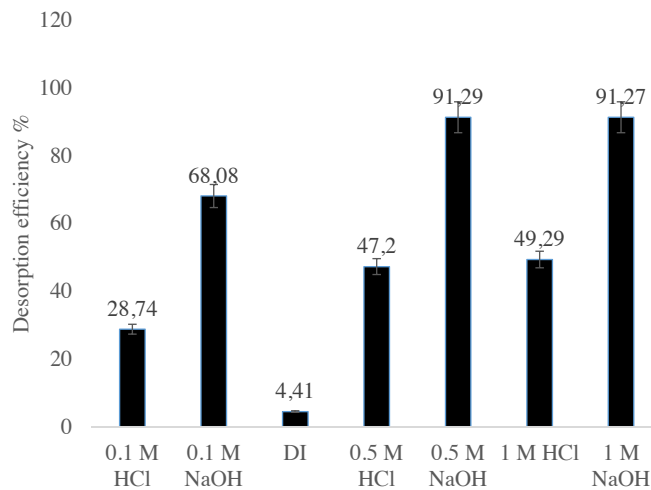


Figure 12. Desorption studies of nanocomposite with Cs⁺ ions.

4. Conclusion

$\text{Fe}_3\text{O}_4/\text{Ch}/\text{HCF}$ nanocomposite was synthesized using Fe_3O_4 obtained using iron ore waste. Temperature, pH value, agitation rate, contact time, adsorbent amount and initial Cs concentration were determined 25 °C, pH: 5, 140 rpm, 30 min, 0.05 g adsorbent and 40 mg/L Cs^+ , respectively. The presence of competitive ions led to a decrease in the amount of Cs adsorbed on nanocomposite, which is due to complexation and nonspecific surface interactions. According to the information obtained from studies with Fe_3O_4 , chitosan and hexacyanoferrates in the literature, iron ions in Fe_3O_4 interact with amino and hydroxyl groups on chitosan and form a core-shell structure with coordination bonds, STPP dissolves in water and forms OH^- and P_3O_5^- ions, and, after that, these ions interact with amine groups of chitosan. It is thought that OH^- and P_3O_5^- , which are formed as a result of the decomposition of STPP and -CN groups in the structure of hexacyanoferrate, interact with iron ions (Fe^{2+} and Fe^{3+}) and keep hexacyanoferrates attached to the core-shell Fe_3O_4 -chitosan composite. It was determined that the adsorption fits the Langmuir isotherm model better and the maximum adsorption capacity is 34.36 mg/g. As the result of the calculation of the thermodynamic parameters, the adsorption enthalpy (ΔH°) is negative, and entropy (ΔS°) is positive as well as the free energy (ΔG°) value is also negative indicates that the adsorption occurs spontaneously at all temperatures.

In the literature, adsorption capacity of various sorbent used on Cs removal is ranging between 6.68 mg g⁻¹ and 306 mg g⁻¹ and illustrated in the table [29–33]; therefore, $\text{Fe}_3\text{O}_4/\text{Ch}/\text{HCF}$ nanocomposite has been used effectively in the removal of Cs from the aqueous medium as well as the reuse of the waste generated in the iron industry. The adsorption process with this nanocomposite can be used as a fast and effective method.

References

1. Kim TY, An SS, Shim WG, Lee JW, Cho SY et al. Adsorption and energetic heterogeneity properties of Cs ions on ion exchange resin. *Journal of Industrial and Engineering Chemistry* 2015; 27: 260-267. doi: 10.1016/j.jiec.2014.12.043
2. Chakraborty D, Maji S, Bandyopadhyay A, Basu S. Biosorption of Cs-137 and strontium-90 by mucilaginous seeds of *Ocimum basilicum*. *Biosource Technology* 2007; 98 (15): 2949-2952. doi: 10.1016/j.biortech.2006.09.035
3. Grossmann R, Maier HJ, Friebel HU, Frischke D. Preparation of radioactive targets for tandem accelerator experiments by high vacuum evaporation–condensation. *Nuclear Instruments and Methods in Physics Research A* 2002; 480 (1): 209-213. doi: 10.1016/S0168-9002(01)02093-9
4. Kim K, Kim K, Choi M, Son SH, Han JH. Treatment of ion exchange resins used in nuclear power plants by super- and sub-critical water oxidation –A road to commercial plant from bench-scale facility. *Chemical Engineering Journal* 2012; 189-190: 213-221. doi: 10.1016/j.cej.2012.02.060
5. Larlus O, Valtchev VP. Crystal Morphology Control of LTL-Type Zeolite Crystals. *Chemistry of Materials* 2004; 16 (17): 3381-3389. doi: 10.1021/cm0498741
6. Abdel Moamen OA, Ibrahim HA, Abdelmonem N, Ismail IM. Thermodynamic analysis for the sorptive removal of Cs and strontium ions onto synthesized magnetic nano zeolite. *Microporous and Mesoporous Materials* 2016; 223: 187-195. doi: 10.1016/j.micromeso.2015.11.009
7. Ambashta RD, Sillanpää M. Water purification using magnetic assistance: A review. *Journal of Hazardous Materials* 2010; 180 (1-3): 38-49. doi: 10.1016/j.jhazmat.2010.04.105
8. Yan F, Sun L, Li F, Zhuang J, Wang H et al. Mesoporous silica-coated superparamagnetic particles prepared by pseudomorphic transformation and their application in purification of plasmid DNA. *Journal of Nanoarticle Research* 2011; 13 (12): 6613-6620. doi: 10.1007/s11051-011-0569-7
9. Naeimi S, Faghiehian H. Performance of novel adsorbent prepared by magnetic metal-organic framework (MOF) modified by potassium nickel hexacyanoferrate for removal of Cs^+ from aqueous solution. *Separation and Purification Technology* 2017; 175: 255-265. doi: 10.1016/j.seppur.2016.11.028
10. Dechojarassri D, Asaina S, Omote S, Nishida K, Furuike T et al. Adsorption and desorption behaviors of Cs on rayon fibers coated with chitosan immobilized with Prussian blue. *International Journal of Biological Macromolecules* 2017; 104: 1509-1516. doi: 10.1016/j.ijbiomac.2017.03.056
11. Alves NM, Mano JF. Chitosan derivatives obtained by chemical modifications for biomedical and environmental applications. *International Journal of Biological macromolecules* 2008; 43 (5): 401-414. doi: 10.1016/j.ijbiomac.2008.09.007
12. Venkatesan J, Bhatnagar I, Kim S. Chitosan-Alginate biocomposite containing fucoidan for bone tissue engineering. *Marine Drugs* 2014; 12 (1): 300-316. doi: 10.3390/md12010300

13. Mujeeb Rahman P, Abdul Mujeeb VM, Muraleedharan K, Thomas SK. Chitosan/nano ZnO composite films: Enhanced mechanical, antimicrobial and dielectric properties. *Arabian Journal of Chemistry* 2018; 11 (1): 120-127. doi: 10.1016/j.arabjc.2016.09.008
14. Chen Y, Wang J. Removal of radionuclide Sr²⁺ ions from aqueous solution using synthesized magnetic chitosan beads. *Nuclear Engineering and Design* 2012; 242: 445-451. doi: 10.1016/j.nucengdes.2011.10.059
15. Kheirandish S, Ghaedi M, Dashtian K, Heidari F, Pourebrahim F et al. Chitosan extraction from lobster shells and its grafted with functionalized MWCNT for simultaneous removal of Pb²⁺ ions and eriochrome cyanine R dye after their complexation. *International Journal of Biological macromolecules* 2017; 102: 181-191. doi: 10.1016/j.ijbiomac.2017.03.035
16. Wang J, Chen C. Chitosan-based biosorbents: Modification and application for biosorption of heavy metals and radionuclides. *Biosource Technology* 2014; 160: 129-141. doi: 10.1016/j.biortech.2013.12.110
17. Guibal E, Elwakeel KZ, Atia AA. Fast removal of uranium from aqueous solution using tetraethylenepentamine modified magnetic chitosan resin. *Biosource Technology* 2014; 160: 107-114. doi: 10.1016/j.biortech.2014.01.037
18. Guibal E, Hamza MF, Fouda A, Elwakeel KZ, Wei Y. Phosphorilation of Guar Gum/Magnetite/Chitosan Nanocomposites for Uranium (VI) Sorption and Antibacterial Applications. *Molecules* 2021; 26: 1920. doi: 10.3390/molecules26071920
19. Atia A, Elwakeel KZ. Uptake of U(VI) from aqueous media by magnetic Schiff's base chitosan composite. *Journal of Cleaner Production* 2014; 70: 292-302. doi: 10.1016/j.clepro.2014.02.017
20. Parajuli D, Takahashi A, Noguchi H, Kitajima A, Tanaka H et al. Comparative study of the factors associated with the application of metal hexacyanoferrates for environmental Cs decontamination. *Chemical Engineering Journal* 2016; 283: 1322-1328. doi: 10.1016/j.cej.2015.08.076
21. Sheha RR. Synthesis and characterization of magnetic hexacyanoferrate (II) polymeric nanocomposite for separation of Cs from radioactive waste solutions. *Journal of Colloid and Interface Science* 2012; 388 (1): 21-30. doi: 10.1016/j.jcis.2012.08.042
22. Arora S, Lal S, Kumar S, Kumar M, Kumar M. Comparative degradation kinetic studies of three biopolymers: Chitin, chitosan and cellulose. *Archives of Applied Science Research* 2011; 3 (3): 188-201.
23. Cao C, Xiao L, Chen C, Shi X, Cao Q et al. In situ preparation of magnetic Fe₃O₄/chitosan nanoparticles via a novel reduction-precipitation method and their application in adsorption of reactive azo dye. *Powder Technology* 2014; 260: 90-97. doi: 10.1016/j.powtec.2014.03.025
24. Bezdorozhev O, Kolodiazhnyi T, Vasyukiv O. Precipitation synthesis and magnetic properties of self-assembled magnetite-chitosan nanostructures. *Journal of Magnetism and Magnetic Materials* 2017; 428: 406-411. doi: 10.1016/j.jmmm.2016.12.048
25. Zhang W, Jia S, Wu Q, Wu S, Ran J et al. Studies of the magnetic field intensity on the synthesis of chitosan-coated magnetite nanocomposites by co-precipitation method. *Materials Science and Engineering C* 2012; 32 (2): 381-384. doi: 10.1016/j.msec.2011.11.010
26. Bhumkar DR, Pokharkar VB. Studies on Effect of pH on Cross-linking of Chitosan With Sodium Tripolyphosphate: A Technical Note. *American Association of Pharmaceutical Scientists* 2006; 7 (2): E138-E143. doi: 10.1208/pt070250
27. Lima E, Hosseini-Bandegharaei A, Moreno-Pirajan J, Anastopoulos I. A critical review of estimation of the thermodynamic parameters on adsorption equilibria. Wrong use of equilibrium constant in the Van't Hoff equation for calculation of thermodynamic parameters of adsorption. *Journal of Molecular Liquids* 2019; 273: 425-434. doi: 10.1016/j.molliq.2018.10.048
28. Mahdi Z, Yu QJ, Hanandeh AE. Removal of lead (II) from aqueous solution using date seed-derived biochar: batch and column studies. *Applied Water Science* 2018; 8:181. doi: 10.1007/s13201-018-0829-0
29. Kim J, Lee S, Jeon C. Adsorption characteristics of sericite for Cs ions from an aqueous solution. *Chemical Engineering and Design* 2014; 92(2): 368-374. doi: 10.1016/j.chemd.2013.07.020
30. Khandaker S, Kuba T, Kamida S, Uchikawa Y. Adsorption of Cs from aqueous solution by raw and concentrated nitric acid-modified bamboo charcoal. *Journal of Environmental Chemical Engineering* 2017; 5 (2): 1456-1464. doi: 10.1016/j.jece.2017.02.014
31. Lee K, Park M, Kim J, Oh M, Lee E et al. Equilibrium, kinetic and thermodynamic study of Cs adsorption onto nanocrystalline mordenite from high-salt solution. *Chemosphere* 2016; 150: 765-771. doi: 10.1016/j.chemosphere.2015.11.072
32. Park S, Lee K, Park C, Hwang K. Highly efficient removal of radioactive Cs by sodium-copper hexacyanoferrate-modified magnetic nanoparticles. *Colloids and Surfaces A Physicochemical and Engineering Aspects* 2017; 516: 375-382. doi: 10.1016/j.colsurfa.2016.12.052
33. Zhao X, Zhang H, Wei J, Li F. Removal of Cs from low-level radioactive wastewaters using magnetic potassium titanium hexacyanoferrate. *Chemical Engineering Journal* 2015; 275 (C): 262-270. doi: 10.1016/j.cej.2015.04.052

Figure S1. Freundlich isotherm graph obtained from cesium adsorption

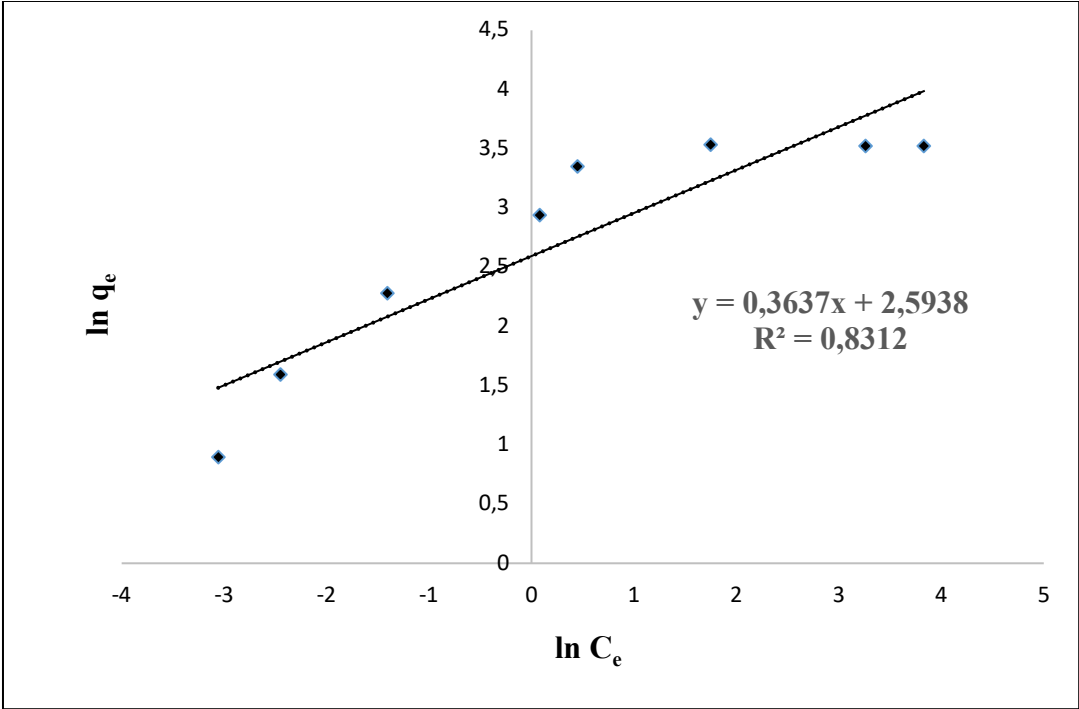


Figure S2. Langmuir isotherm graph obtained from cesium adsorption

